applied sciences

MDPI

Article

Optical Conveyor Belts for Chiral Discrimination: Influence of De-Phasing Parameter

Luis Carretero *,†, **Pablo Acebal** † and **Salvador Blaya** †

Departamento de Ciencia de Materiales, Óptica y Tecnología Electrónica, Universidad Miguel Hernández, Avda. de la Universidad, 03202 Elche, Spain; pablo@dite.umh.es (P.A.); salva@dite.umh.es (S.B.)
* Correspondence: l.carretero@umh.es
† These authors contributed equally to this work.

Received: 26 February 2019; Accepted: 23 March 2019; Published: 28 March 2019

Featured Application: The results of this work could be applied to obtain enantiomeric separation by using electromagnetic fields.

Abstract: A numerical analysis is carried out of the influence of the de-phasing parameter of an optical conveyor belt in the enantiomeric separation. The optical conveyor belt is obtained by the interference of a Laguerre Gaussian and a Gaussian beam with different beam waists, which are temporally de-phased. In order to obtain the maximum separation distance between enantiomers, we calculate the optimum range of values of the de-phasing parameter.

Keywords: optical conveyor belt; chiral particle; vortex beams; Rayleigh particles

1. Introduction

One important task in biology is the separation of enantiomers, which can be achieved by using different techniques such as gas chromatography, high performance liquid chromatography, or capillary electrophoresis [1]. Different groups [2–5] have recently analyzed the use of optical fields to generate enantiomeric separation. In this sense, a study has been made of lateral optical forces (LOF) generated by interfering plane waves [6] in order to obtain chirality sorting, and the LOF effect on paired chiral particles has also been discussed [7]. Furthermore, another way of generating LOF is given by evanescent waves, which transport spin angular momentum and could be used for chirality sorting [3]. Thus, micro-metric particles have been sorted in a fluidic medium by using the spin-dependent optical forces of chiral particles [8]. Moreover, our group has demonstrated that it is possible to obtain chiral resolution of nanoparticles by using an optical conveyor belt [9–12] through the superposition of two orthogonal counter-propagating temporally-de-phased beams [13,14]. In this paper, we are going to analyze the effects of the temporal de-phasing parameter on the chiral resolution of the optical conveyor belt, showing that the maximum separation distance between enantiomers can be obtained by selecting the correct range of the de-phased parameter. Finally, the dynamics of enantiomers are studied in their final trap region.

2. Results

2.1. Optical Forces

In order to analyze particle dynamics, we have solved the overdamped Langevin equation [15]:

$$\vec{F}(\vec{R}(t)) - \gamma \frac{d\vec{R}}{dt} + \vec{\mathcal{F}}(t) = 0 \quad (1)$$

where $\vec{F}(\vec{R}(t))$ is the optical force, $\vec{R}(t)$ is the position vector of the particle at time t, $-\gamma\frac{d\vec{R}}{dt}$ is the frictional force of a particle, and $\vec{\mathcal{F}}(t)$ is a random function force with time that we have assumed null (the Brownian effect is not taken into account). Coefficient $\gamma = 6\pi\eta_v a$, where η_v is the viscosity of the medium (water in our case) and parameter a is the particle radius. We consider small chiral particles with radius a much lower than the wavelength of the electromagnetic field $\vec{E}$, $\vec{H}$, inside a dielectric medium of refractive index n. The optical force on the chiral sphere (CS) can be deduced by using the dipole approximation for which CS is modeled as an induced magnetic ($\vec{m}$) and electric dipole ($\vec{p}$) given by [16]:

$$\begin{aligned}
\vec{m} &= 4\pi(-i\,\frac{\alpha_{em}}{\eta}\vec{E} + \alpha_{mm}\vec{H}) \\
\vec{p} &= 4\pi\epsilon_0(\alpha_{ee}\vec{E} + i\,\alpha_{em}\eta\vec{H})
\end{aligned} \tag{2}$$

where $\vec{H}$ and $\vec{E}$ are the magnetic and electric fields, α_{ee}, α_{mm}, and α_{em} are the electric, magnetic, and chiral polarizability, respectively, η is the vacuum impedance, and ϵ_0 is the permittivity of free space. In the case of Rayleigh particles with a small chirality parameter δ (it is assumed that the refractive index of the chiral particle is given by $n_{LR} = np \pm \delta$, where $n_L = np + \delta$ defines the refractive index for the left-handed enantiomer and $n_R = np + \delta$ for the right-handed one), the electric, magnetic, and chiral polarizability can be written (in absence of absorption) as [3,16]:

$$\begin{aligned}
\alpha_{ee} &= n^2\,a^3\,\frac{n_p^2 - n^2}{n_p^2 + 2n^2} \\
\alpha_{mm} &= 0 \\
\alpha_{em} &= -a^3\,\frac{(\pm\,\delta\,n^2)}{n_p^2 + 2n^2}
\end{aligned} \tag{3}$$

These expressions have been obtained by taking into account that the chirality parameter $|\delta| << 1$, which implies that in the dipolar limit, all magnetic parts (α_{mm} is proportional to δ^2) of force can be disregarded [2]. The electric energy density (U_e) and the helicity density (U_h) can be defined as:

$$U_e = \frac{\epsilon_0\epsilon_r}{4}|\vec{E}|^2 \tag{4}$$

$$U_h = \frac{\epsilon_0\mu_0}{2\,k_0}\Im(\vec{E}.\vec{H}^*) \tag{5}$$

where $\Im$ and $*$ denote the imaginary part and the complex conjugate respectively, ϵ_r is the relative permittivity of the medium in which the particle is immersed, and k_0 is the wavenumber. Due to the electric density energy U_e and helicity density U_h, the particle is subject to a potential energy W given by:

$$W = \pi\epsilon_0\alpha_{ee}|\vec{E}|^2 - 2\pi\epsilon_0\eta\alpha_{em}\Im(\vec{E}.\vec{H}^*) \tag{6}$$

In the Rayleigh regime, the optical force $\vec{F}(\vec{R}(t))$, described by Equation (1), exerted upon the chiral spheres by the electromagnetic field, can be approximated to a gradient force [4,17]:

$$\vec{F}(\vec{R}(t)) = \nabla W \tag{7}$$

2.2. Electromagnetic Field

Let us consider two counter-propagating Gaussian and Laguerre-Gaussian beams (LGB) [13], whose electric fields $(\vec{e}_0, \vec{e}_1)$ are elliptically polarized, slightly temporally de-phased $(\tau\, t)$, and with different beam waist:

$$\vec{e}_0 = G_0(x,y,z)\, exp(i\,(\phi_0(x,y,z) + \tau\, t))(\hat{x} + b_0\, i\hat{y}) \tag{8}$$

$$\vec{e}_1 = G_1(x,y,z)\, exp(i\,(\phi_1(x,y,z))(\hat{x} + b_1\, i\hat{y}) \tag{9}$$

The total electric field may be written as:

$$\vec{E} = \vec{e}_0 + \vec{e}_1 \tag{10}$$

introducing cylindrical coordinates $r = \sqrt{x^2 + y^2}$ and $\theta = arctan(\frac{y}{x})$, the amplitude and phase of the fields $(\vec{e}_0, \vec{e}_1)$ given by Equations (8) and (9) can be expressed (assuming a (1-1) Laguerre Gaussian beam) as:

$$G_0(r,\theta,z) = A_0 \frac{w_0}{w_0(z)} exp\left(-\frac{r^2}{w_0^2(z)}\right) \tag{11}$$

$$G_1(r,\theta,z) = A_0 \frac{w_1}{w_1(z)} \left(\frac{\sqrt{2}r}{w_q(z)}\right) exp\left(-\frac{r^2}{w_1^2(z)}\right) L_1^1\left(\frac{2r^2}{w_1^2(z)}\right) \tag{12}$$

$$\phi_0(r,\theta,z) = -k\left(\frac{r^2}{2R_0(z)} + z\right) + \zeta_0(z) \tag{13}$$

$$\phi_1(r,\theta,z) = k\left(\frac{r^2}{2R_1(z)} + z\right) + \theta - 4\zeta_1(z) \tag{14}$$

where L_1^1 is the generalized Laguerre (1,1) polynomial, $k = n\frac{\omega}{c}$ is the wave number inside of a dielectric medium of refractive index n, and A_0, $w_q(z)$, $\zeta_q(z)$, and $R_q(z)$ are the electric field amplitude, beam waist, the Gouy phase, and the curvature radius of Gaussian wave fronts for $q \in \{0,1\}$, respectively [18]. These parameters are given by:

$$w_q(z) = w_q \sqrt{1 + \frac{z^2}{z_q^2}} \tag{15}$$

$$R_q(z) = z\left(1 + \frac{z_q^2}{z^2}\right) \tag{16}$$

$$\zeta_q(z) = tan^{-1}\left(\frac{z}{z_q}\right) \tag{17}$$

$$z_q = \frac{\pi\, w_q^2\, n}{\lambda_0} \tag{18}$$

where λ_0 is the vacuum wavelength. The magnetic field according to the Maxwell equations is given by:

$$\nabla \times \vec{E} = i\omega_0\mu_0\vec{H} \tag{19}$$

ω_0 being the electromagnetic field frequency.

Under the condition $b_0 = -b_1^{-1}$, the polarization of the counter-propagating beams will be right-handed and left-handed, respectively, the degree of circular polarization being different from one if $b_1 \neq 1$. In this case, Equation (6) can be written as:

$$W(r,\theta,z) = W_0(r,z) + W_c(r,z)\, cos(\tau\, t + \phi_0 - \phi_1) + W_s(r,z) sin(\tau\, t + \phi_0 - \phi_1) \tag{20}$$

where:

$$W_0(r,z) = \frac{\pi\epsilon_0}{b_1^2 k_0}\left(G_0^2\left((1+b_1^2)k_0\alpha_{ee} + 4b_1\alpha_{em}\partial_z\phi_0\right) + b_1^2 G_1^2\left((1+b_1^2)k_0\alpha_{ee} - 4b_1\alpha_{em}\partial_z\phi_1\right)\right) \quad (21)$$

$$W_s(r,z) = -\frac{2(b_1^2-1)\pi\epsilon_0\alpha_{em}}{b_1 k_0}(G_1\,\partial_z G_0 - G_0\,\partial_z G_1) \quad (22)$$

$$W_c(r,z) = -\frac{2(b_1^2-1)\pi\epsilon_0\alpha_{em}}{b_1 k_0} G_0\, G_1(\partial_z\phi_0 + \partial_z\phi_1) \quad (23)$$

Taking into account that $\phi_0 - \phi_1 \approx -2kz - \theta$, Equation (20) can therefore be written as:

$$W = W_0(r,z) + W_s(r,z)sin(\phi(z,\theta)) + W_c(r,z)cos(\phi(z,\theta)) \quad (24)$$

where $\phi(z,\theta) = \tau\, t - 2k\, z - \theta$. Equation (24) describes a chiral-dielectric optical trap given by $W_0(r,z)$ and a chiral conveyor given by $W_s(r,z)\, sin(\tau\, t - 2k\, z - \theta) + W_c(r,z)cos(\tau\, t - 2k\, z - \theta)$.

By introducing Equation (24) into Equations (7) and (1), we obtain the following dynamic equations for chiral particles:

$$\gamma\dot{r} = \partial_r W_0(r,z) + \partial_r W_s(r,z)sin(\phi(z,\theta)) + \partial_r W_c(r,z)cos(\phi(z,\theta)) \quad (25)$$

$$\gamma r\dot{\theta} = \frac{-W_s(r,z)cos(\phi(z,\theta)) + W_c(r,z)sin(\phi(z,\theta))}{r} \quad (26)$$

$$\begin{aligned}\gamma\dot{z} \;&=\; \partial_z W_0(r,z) + (\partial_z W_s(r,z) + 2kW_c(r,z))sin(\phi(z,\theta)) \\ &\quad +(\partial_z W_c(r,z) - 2kW_s(r,z))cos(\phi(z,\theta))\end{aligned} \quad (27)$$

It is important to note that in Equation (25), $\partial_r W_0(r,z) >> \partial_r W_s(r,z) >> \partial_r W_c(r,z)$ and in Equation (27), $-2kW_s(r,z) >> \partial_z W_s(r,z); 2kW_c(r,z) >> \partial_z W_c(r,z)$, so the dynamic equations of chiral particles can be approximated to:

$$\gamma\dot{r} = \partial_r W_0(r,z) \quad (28)$$

$$\gamma r\dot{\theta} = \frac{-W_s(r,z)cos(\tau\, t - 2k\, z - \theta) + W_c(r,z)sin(\phi(z,\theta))}{r} \quad (29)$$

$$\gamma\dot{z} = \partial_z W_0(r,z) - 2kW_s(r,z)cos(\tau\, t - 2k\, z - \theta) + 2kW_c(r,z)sin(\tau\, t - 2k\, z - \theta) \quad (30)$$

Equation (28) shows that chiral particles are trapped in the radial positions r_p where the function $W_0(r,z)$ is maximum ($\dot{r} = \frac{\partial W_0}{\partial r}|_{r=r_p} = 0$). Equations (26) and (27) imply that chiral particles describe helical trajectories similar to those obtained in the case of dielectric particles [19].

3. Discussion

In the numerical calculation, we have used the values of $\lambda = 1070$ nm, $a = \lambda/15$, $n_p = 1.45$, $n = 1.33$, $w_0 = 5\lambda$, $w_1 = 4\lambda$, $b_1 = 0.9$, $\delta = \pm 0.06$, and $A_0 = 2 \times 10^8$ V/m assuming that the initial position of the enantiomers is $r_0 = 3\lambda, \theta_0 = 0, z_0 = 10\lambda$. Figure 1 shows the potential energy W(r,z) given by Equation (20). As can be observed, W shows a maximum at radial position $r_p = 1.6\lambda$ (green dashed line), which is the radial coordinate where particles will be initially trapped according to Equation (28).

Thus, by using the indicated fixed values, the chiral conveyor is mainly controlled by the de-phase τ, which governs the conveyor velocity. In fact, if $\tau = 0$, there will not be any temporal dependence in Equations (29) and (30), and there will not be a chiral conveyor; consequently, W will act like a chiral trap.

In this case, both enantiomers will be trapped in the same region, as shown in Figure 2a, and as a result, there is no effective enantiomeric separation. Figure 2b–f shows the enantiomeric separation produced by the action of the chiral optical conveyor described by Equations (1), (7), and (25)–(27).

As can be observed, the particle trajectories are spiral in all cases, the pitch and velocity of optical conveyors being strongly dependent on de-phase parameter τ [19]. In this sense, the behavior of chiral conveyors is very similar to dielectric conveyors, and the main difference from the results obtained in [19] is that the movement of particles in the z direction is limited due to the axial dependence of parameters $W_0(r,z)$ and $W_s(r,z)$. Furthermore, as can be seen in Figure 2, on increasing τ, the enantiomeric separation also increases until it reaches a maximum separation that slowly decreases for high values of de-phase τ.

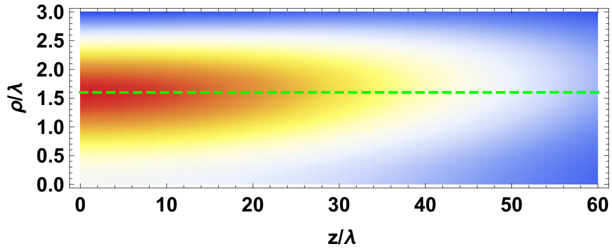

Figure 1. Potential energy W(r,z) for parameters: $\lambda = 1070$ nm, $a = \lambda/15$, $n_p = 1.45$, $n = 1.33$, $w_0 = 5\lambda$, $w_1 = 4\lambda$, $b_1 = 0.9$, $\delta = \pm 0.06$, and $A_0 = 2 \times 10^8$ V/m.

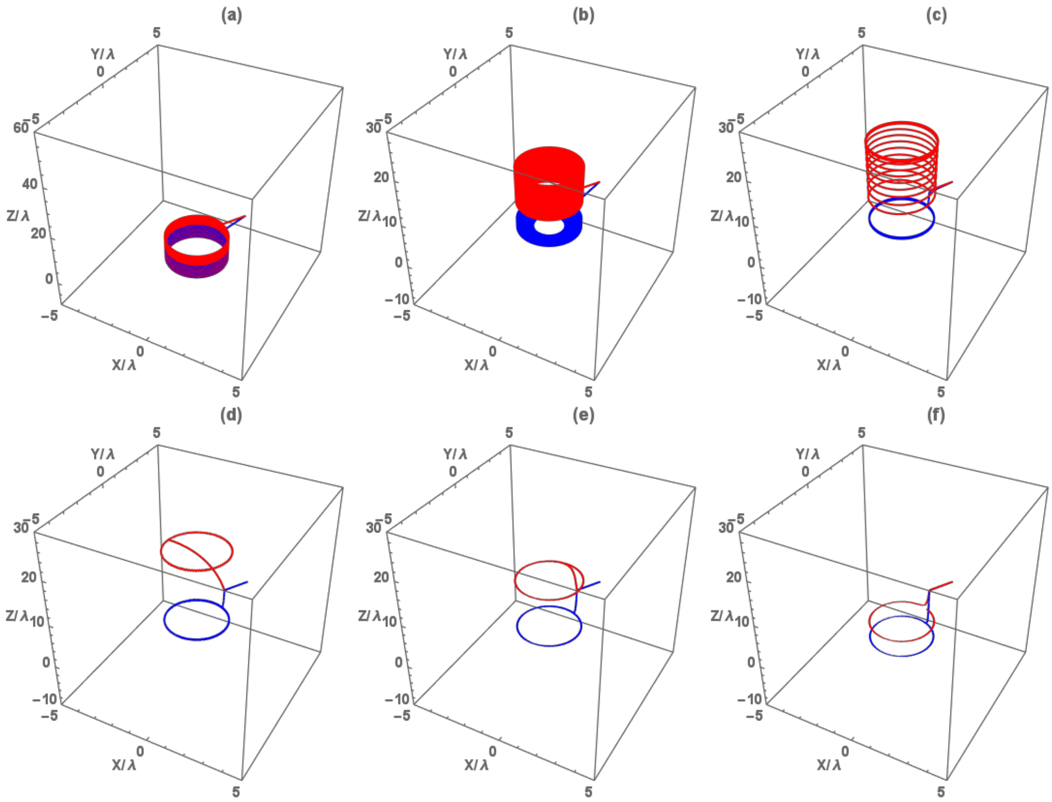

Figure 2. Particle trajectories for different τ values and for both enantiomers ($\delta > 0$ blue and $\delta < 0$ red). (**a**) $\tau = 0$ Hz, (**b**) $\tau = 2$ Hz, (**c**) $\tau = 10$ Hz, (**d**) $\tau = 500$ Hz, (**e**) $\tau = 1$ kHz, and (**f**) $\tau = 5$ kHz.

This result can be clarified in Figure 3, where the behavior of enantiomeric separation (Δ, defined as the axial distance between trapped enantiomers) is represented as a function of τ. As previously mentioned, there is a fast increment of Δ when τ rises, obtaining a maximum value of 18λ for $\tau = 10$ Hz, which remains nearly constant (see the inset graphics in Figure 3), until reaching a value of $\tau = 100$ Hz to decrease slowly subsequently.

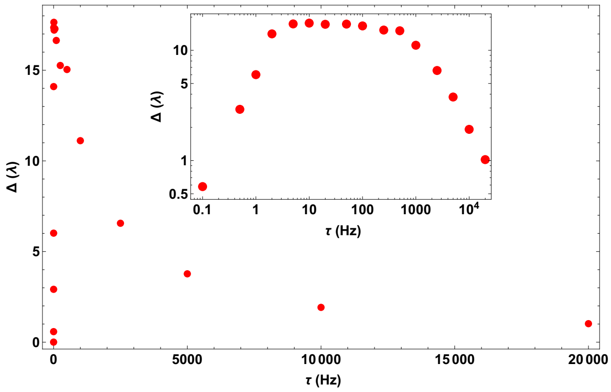

Figure 3. Enantiomeric separation versus τ. The inset figure shows enantiomeric separation versus τ in the logarithmic scale.

Figure 4 shows the particles position at different times for a de-phase parameter $\tau = 10$ Hz. As can be observed in Figure 4a, enantiomers are trapped at $r = r_p$ in different z positions in a short time ($t = 0.01$ s). Figure 4b–d shows that positive enantiomers ($\delta > 0$) are trapped more quickly than negative ones. It can also be observed in Figure 4b–e that there are two traps, but at the end ($t = 10$ s), only one of them is stable for each enantiomer.

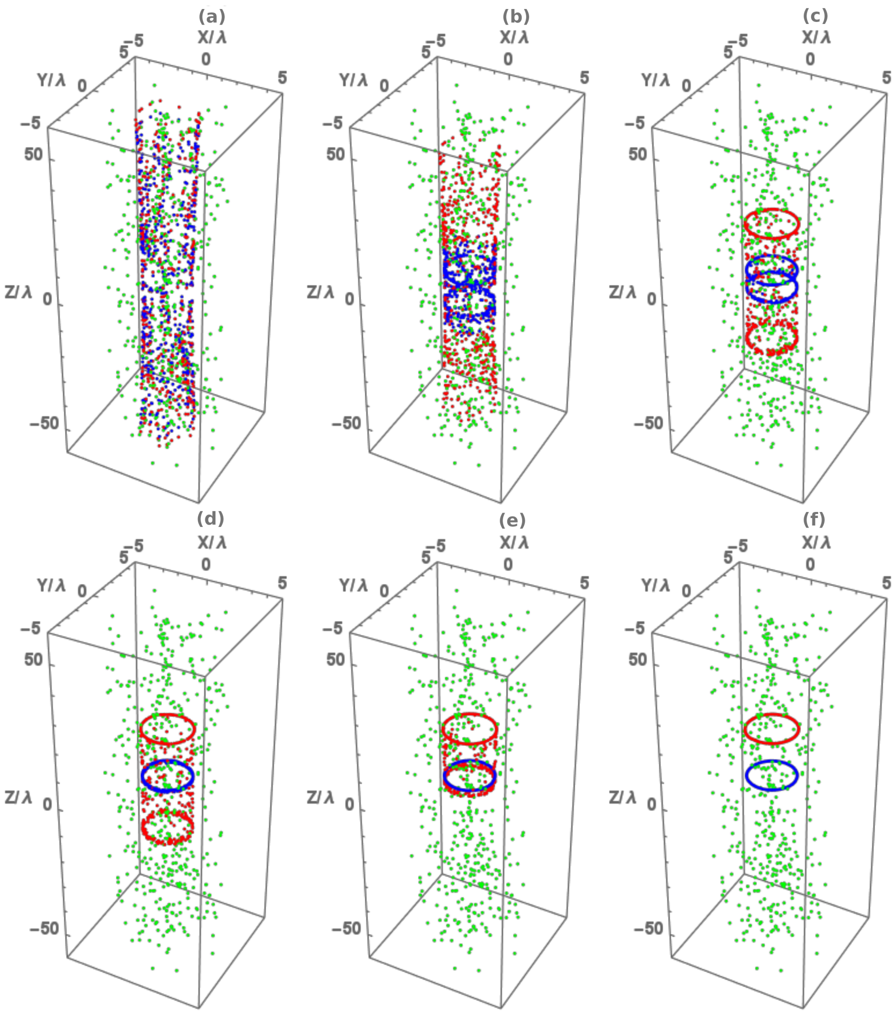

Figure 4. Particles' position at different times: (**a**) $t = 0.01$ s, (**b**) $\tau = 0.1$ s, (**c**) $t = 1$ s, (**d**) $t = 2$ s, (**e**) $t = 5$ s, and (**f**) $t = 10$ s, for $\tau = 10$ Hz ($\delta > 0$ blue and $\delta < 0$ red; green dots show the initial particles' position).

It is interesting to note that when enantiomers are finally trapped at different z positions (see Figures 2 and 4f), they describe circular trajectories with angular frequencies ω, which are shown in Figure 5.

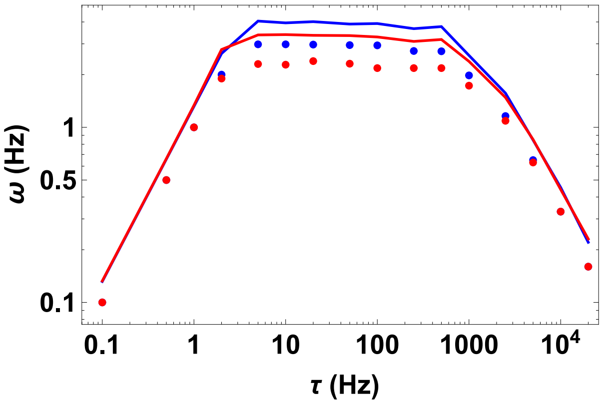

Figure 5. Angular frequency of the last circular trajectory of trapped enantiomers ($\delta > 0$ blue and $\delta < 0$ red) versus τ (the continuous line shows the predicted results from Equation (34)).

As can be observed in Figure 5, at low and high τ values, the frequency of the circular trajectories ω shows similar values for both enantiomers (1 kHz $< \omega <$ 1 Hz). However, for τ values between 1 and 1000 Hz, the frequency ω is nearly constant and equal to 2 Hz for enantiomers with $\delta < 0$ and 3 Hz in the case of $\delta > 0$. One explanation for this result could be that, at the final time, particles describe a limit cycle in which $z(t)$ reaches a limit value $z^{\tau}_{\pm\delta}$ (each enantiomer goes to a final z position that depends on their value $\pm\delta$ and de-phase τ) at the fixed value $r = r_p$ (see Figure 2). In this case (when the limit cycle is reached $z = z^{\tau}_{\pm\delta}$, $r = r_p$), Equations (28) and (30) can be approximated to:

$$\dot{r} \approx 0 \implies r = r_p \tag{31}$$

$$\gamma r_p \dot{\theta} \approx \frac{-W_s(r_p, z^{\tau}_{\pm\delta}) cos(\tau\, t - 2k\, z^{\tau}_{\pm\delta} - \theta) + W_c(r_p, z^{\tau}_{\pm\delta}) sin(\tau\, t - 2k\, z^{\tau}_{\pm\delta} - \theta)}{r_p} \tag{32}$$

$$\dot{z} \approx 0 \implies$$
$$-W_s(r_p, z^{\tau}_{\pm\delta}) cos(\tau\, t - 2k\, z^{\tau}_{\pm\delta} - \theta) + W_c(r_p, z^{\tau}_{\pm\delta}) sin(\tau\, t - 2k\, z^{\tau}_{\pm\delta} - \theta) = \frac{\partial_z W_0(r,z)|_{(r_p, z^{\tau}_{\pm\delta})}}{2k} \tag{33}$$

Introducing Equation (33) into (32), we finally obtain that:

$$\dot{\theta} \approx (-2\, k\, r_p^2\, \gamma)^{-1}\, \partial_z W_0(r,z)|_{(r_p, z^{\tau}_{\pm\delta})} = \omega \tag{34}$$

As can be observed in Figure 5, the approximated function (34) qualitatively explains the final frequency values ω, although quantitatively, the predictions are overestimated be approximately 1 Hz.

A possible explanation for this observed overestimation is that we have used the approximations:

$$(\partial_z W_s(r,z) + 2kW_c(r,z)) sin(\phi(z,\theta)) \approx 2kW_c(r,z) sin(\phi(z,\theta))$$
$$(\partial_z W_c(r,z) - 2kW_s(r,z)) cos(\phi(z,\theta)) \approx -2kW_s(r,z) cos(\phi(z,\theta))$$

in order to obtain the analytical approximated Equation (34).

Finally, Figure 6 shows the particle separation of particles with different chiral parameter δ when we use the de-phasing parameter $\tau = 10$ Hz, taking in all cases a final time of 50 s.

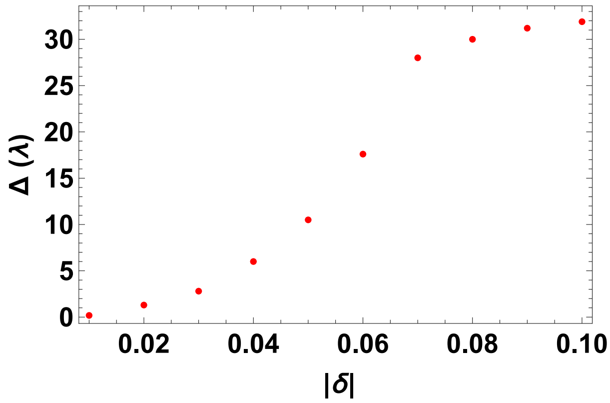

Figure 6. Particle separation of particles with different chiral parameter δ, when we use the de-phasing parameter $\tau = 10$ Hz, taking in all cases a final time of 50 s.

As can be observed, the particle separation is null for low values of δ, increasing for higher values of δ until reaching a saturation zone for a fixed time of 50 s. It is important to note that at this time, particles with $\delta > 0.7$ have not reached their limit cycle.

4. Conclusions

We have demonstrated that the role of the de-phasing parameter in an optical conveyor is critical for chiral separation results. We have presented a range of values for such a parameter where maximum enantiomeric discrimination is reached. We have also shown that particles reach a limit cycle in which they describe circular trajectories with a constant angular frequency, which can be analytically estimated with dynamic equations in the limit cycle.

Author Contributions: Conceptualization, L.C. and P.A.; methodology, S.B.; software, L.C.; investigation, L.C., P.A. and S.B.; writing, original draft preparation, L.C.

Funding: This research received no external funding.

Conflicts of Interest: The authors declare no conflict of interest.

References

1. Gubitz, G.; Schmidt, M.G. (Eds.) *Chiral Separations. Methods and Protocols*; Humana Press: New York, NY, USA, 2004.
2. Canaguier-Durand, A.; Hutchison, J.A.; Genet, C.; Ebbesen, T.W. Mechanical separation of chiral dipoles by chiral light. *New J. Phys.* **2013**, *15*, 123037.
3. Hayat, A.; Mueller, J.P.B.; Capasso, F. Lateral chirality-sorting optical forces. *Proc. Natl. Acad. Sci. USA* **2015**, *112*, 13190–13194. [CrossRef] [PubMed]
4. Cameron, R.P.; Barnett, S.M.; Yao, A.M. Discriminatory optical force for chiral molecules. *New J. Phys.* **2014**, *16*, 013020. [CrossRef]
5. Bradshaw, D.S.; Forbes, K.A.; Leeder, J.M.; Andrews, D.L. Chirality in Optical Trapping and Optical Binding. *Photonics* **2015**, *2*, 483–497. [CrossRef]
6. Chen, H.; Liang, C.; Liu, S.; Lin, Z. Chirality sorting using two-wave-interference induced lateral optical force. *Phys. Rev. A* **2016**, *93*, 053833. [CrossRef]
7. Chen, H.; Jiang, Y.; Wang, N.; Lu, W.; Liu, S.; Lin, Z. Lateral optical force on paired chiral nanoparticles in linearly polarized plane waves. *Opt. Lett.* **2015**, *40*, 5530–5533. [CrossRef]
8. Tkachenko, G.; Brasselet, E. Optofluidic sorting of material chirality by chiral light. *Nat. Commun.* **2014**, *5*, 3577. [CrossRef] [PubMed]
9. Cizmar, T.; Garces-Chavez, V.; Dholakia, K.; Zemanek, P. Optical conveyor belt for delivery submicron objects. *Appl. Phys. Lett.* **2005**, *86*, 174101. [CrossRef]
10. Ruffner, D.B.; Grier, D.G. Optical conveyors: A class of active tractor beams. *Phys. Rev. Lett.* **2012**, *109*, 163903. [CrossRef] [PubMed]

11. Fernandes, D.E.; Silveirinha, M.G. Optical tractor beam with chiral light. *Phys. Rev. A* **2015**, *91*, 061801. [CrossRef]
12. Fernandes, D.E.; Silveirinha, M.G. Single-Beam Optical Conveyor Belt for Chiral Particles. *Phys. Rev. Appl.* **2016**, *6*, 014016. [CrossRef]
13. Carretero, L.; Acebal, P.; Blaya, S. Chiral Rayleigh particles discrimination in dynamic dual optical traps. *J. Quant. Spectrosc. Radiat. Transf.* **2017**, *201*, 209–215. [CrossRef]
14. Acebal, P.; Carretero, L.; Blaya, S. Design of an optical conveyor for selective separation of a mixture of enantiomers. *Opt. Express* **2017**, *25*, 32290–32304. [CrossRef]
15. Reif, F. *Fundamentals of Statistical and Thermal Physics*; McGraw-Hill Book Company: Nong Grove, IL, USA, 1965.
16. Lakhtakia, A.; Varadan, V.K.; Varadan, V.V. Effective properties of a sparse random distribution of non-interacting small chiral spheres in a chiral host medium. *J. Phys. D Appl. Phys.* **1991**, *24*, 1. [CrossRef]
17. Zhao, Y.; Saleh, A.A.E.; Dionne, J.A. Enantioselective Optical Trapping of Chiral Nanoparticles with Plasmonic Tweezers. *ACS Photonics* **2016**, *3*, 304–309. [CrossRef]
18. Saleh, B.E.A.; Teich, M.C. *Fundamentals of Photonics*; Wiley: Hoboken, NJ, USA, 1991.
19. Carretero, L.; Acebal, P.; Garcia, C.; Blaya, S. Helical tractor beam: analytical solution of Rayleigh particle dynamics. *Opt. Express* **2015**, *23*, 20529–20539. [CrossRef] [PubMed]